GE HealthCare

White Paper

A new era of image reconstruction: TrueFidelity DL

Technical white paper on deep learning image reconstruction

Jiang Hsieh, Eugene Liu, Brian Nett, Jie Tang, Jean-Baptiste Thibault, Sonia Sahney

Contents

Introduction

GE HealthCare's deep learning image reconstruction (DLIR) is the first Food and Drug Administration (FDA) cleared technology to utilize a deep neural network-based recon engine to generate high quality TrueFidelity DL computed tomography (CT) images. DLIR opens a new era for CT-image reconstruction by addressing challenges of filtered back-projection (FBP) and iterative reconstruction (IR).

DLIR features a deep neural network (DNN), which was trained with high quality FBP data sets to learn how to differentiate noise from signals, and to intelligently suppress the noise without impacting anatomical and pathological structures.

The resulting TrueFidelity DL CT images, with outstanding image quality and preferred noise texture, have the potential to improve reading confidence in a wide range of clinical applications, including imaging the head, whole body, cardiovascular, and for patients of all ages.
DLIR is designed with fast reconstruction speed for routine CT use, even in acute care settings.

This white paper will: first, take a look at the overall evolution of CT image reconstruction; second, explain the design, supervised training, and deployment of DLIR engine; and third, reveal early phantom and clinical evidence illustrating the performance of TrueFidelity DL on practical cases.

Challenges of Filtered Back-Projection and Iterative Reconstruction

Filtered back-projection (FBP) was the dominant algorithm used in image reconstruction for the first 30 years of CT because of its computational efficiency and accuracy. The algorithm lends itself nicely to parallel processing and allows images to be reconstructed in nearly real time as the patient is being scanned. From an accuracy point of view, the algorithm can reconstruct the "exact" replica of the scanned object when the input sinogram is "ideal." These highly desired properties, however, come with significant limitations. FBP generally fails to model the non-ideal behaviors of the CT system. Departures from ideal behavior can come from the fundamental properties of X-ray physics (e.g., beam hardening and scatter), the statistical nature of the data acquisition (e.g., limited X-ray photon flux and electronic noise), geometric factors of the system (e.g., partial volume or finite X-ray focal spot size and detector cell size), and patient related factors (e.g., patient positioning and motion). These limitations often lead to higher radiation doses for patients in order to get acceptable image quality or result in reconstructed images of limited quality.[1]

To overcome the shortcomings of FBP, iterative reconstruction (IR) was introduced to CT.[2,3] Instead of a closed-form solution as in FBP, IR relies on finding the solutions, which are the reconstructed images that match the reconstruction model in an iterative fashion. Modeling accuracy that drives reconstruction image quality often leads to increased complexity in the IR reconstruction process to approximate the non-ideal behavior of the data acquisition system and often slows down performance. The most comprehensive IR, the so-called model-based iterative reconstruction (MBIR), explicitly accounts for system statistics, X-ray physics, system optics, and patient characteristics all at the same time.[4] To make the solution tractable (i.e. capable of being handled mathematically), the traditional ways of handling these models focus on simplifying complex and often intertwined phenomena with our theoretical understanding of the physics, statistics, image properties, and engineering. This approach manages the optimization of the solution with a limited number of parameters, typically less than a hundred, either calculated or manually tuned.

Although MBIR and IR are quite successful in reducing dose to patients, their performance in terms of image quality may be less than satisfactory under the most difficult conditions. The visual impression of the reconstructed images often differs from the look and feel of images generated with FBP in ideal conditions due to the modeling complexity that the algorithm can manage. It is often reported that the noise texture appears "blotchy," "plastic-looking" or simply "unnatural."[5] The degree of degradation from the expected appearance of a CT image by a trained radiologist is often linked to the strength of the IR algorithm: the stronger the IR, the more "plastic" the image looks. Compromised scanning conditions such as low dose make things worse, forcing the algorithm to work even harder, further degrading image appearance in order to produce results with low noise: non-linearities in the processing result in locally flat regions in homogeneous tissues and residual noise spikes around sharp edges such as bones and vessel boundaries in order to preserve high resolution detail. In routine clinical practice, therefore, radiologists often limit the IR to a level that they are comfortable with. As a result, IR often offers a trade-off between true dose reduction and reading diagnostic confidence.

Filtered Back-Projection (FBP) is accurate when radiation dose is high and the input sinogram is ideal, but in low dose settings, it is challenged with higher image noise and artifacts.

Iterative Reconstruction (IR) is successful in reducing radiation dose, but has image texture challenges with full strength due to limited complexity of the model.

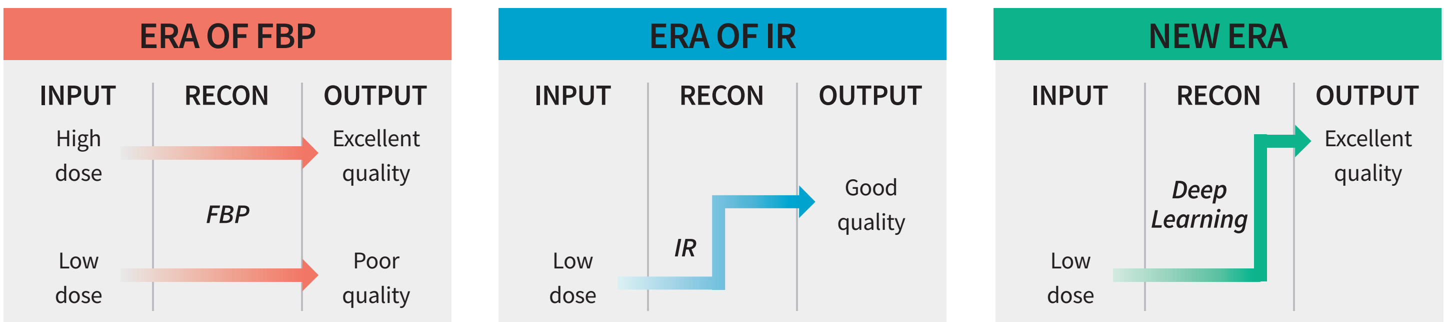

Figure 1: Generations of CT reconstruction technologies. The limitations of FBP and IR motivated GE to explore a new era of deep learning based CT image reconstruction.

The New Era of Deep Learning-Based Image Reconstruction

Faced with these limitations of IR, which was considered the state of the art, the development team at GE asked the following question: are these shortcomings the results of a lack of refinement of the IR technology or the fundamental limitations of a principled approach whereby modeling accuracy drives image quality? For many years, GE was at the forefront of pushing IR modeling further with spectacular results in concurrent noise reduction and spatial resolution performance, yet image texture and general appearance remained compromised relative to ideal expectations.

Perhaps a new technology was needed to break through the modeling limitations of IR itself. Which technology had the potential to overcome this tradeoff? These questions motivated GE to explore deep learning–based image reconstruction (Fig. 1).

Why is Deep Learning so Compelling?

Deep learning (DL) is a subset of machine learning (ML), both of which are subsets of artificial intelligence (AI).[6,7] AI is a broad term to cover the theory and development of computer systems to be able to perform tasks that normally require human intelligence. ML is based on the idea that systems can learn from data, patterns, and features to make decisions with minimal human intervention; and DL utilizes Deep Neural Networks (DNNs) to accomplish the same tasks that ML does. A DNN consists of multiple layers of mathematical equations, and it can find the correct mathematical manipulation to turn the input into the output, whether it be a linear or non-linear relationship.

DL technology has gained significant popularity in recent years because of advances in computational power and the development of modern algorithms for network topology and efficient training. The power of DL lies in its ability to handle complex models and a vast number of parameters far beyond the abilities of human engineers and scientists.[6,7] Traditional algorithms rely on humans to manage parameters so that an optimal solution is tractable. The human-based optimization process limits the number of parameters to be manually optimized to typically less than a hundred. IR is particularly challenged in that regard since a growing number of parameters makes it more difficult to retain the necessary convergence properties of the algorithm. This limits the complexity of the models that can be incorporated into the iterative reconstruction process and, eventually, limits the overall performance of the algorithm. However, a DL approach does not require explicit models for the real system to be simplified to a few parameters. These models can be formed directly by the training process, with a significantly higher number of dimensions, and a number of parameters that can be handled in the millions, because computers can be used to train them concurrently.

With appropriate network topology, a DL model can embody and represent the most complex relationships in a manner so far unattainable with conventional modeling approaches. DL thereby avoids many of the pitfalls of traditional algorithms and lends itself nicely to solving the fundamental challenges of IR. This led GE HealthCare to the creation of a deep learning-based image reconstruction engine.

With the ability to handle complex models and a vast number of parameters through training process, deep learning holds the promise of solving the fundamental challenges of Iterative Reconstruction.

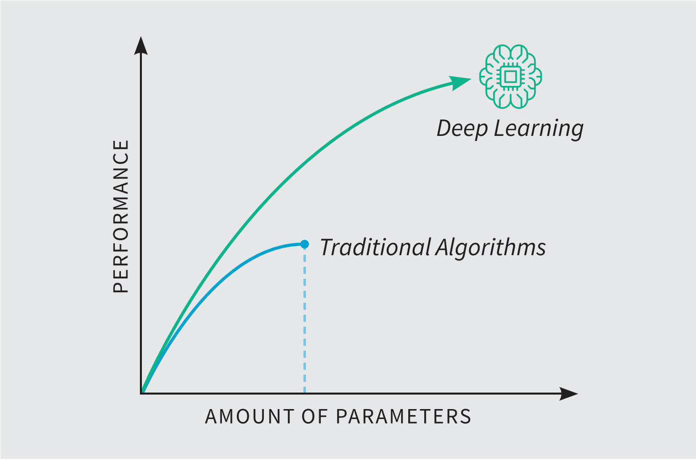

Figure 3: Deep learning outperforms the traditional algorithms that are limited by the number of models and parameters they can manage.

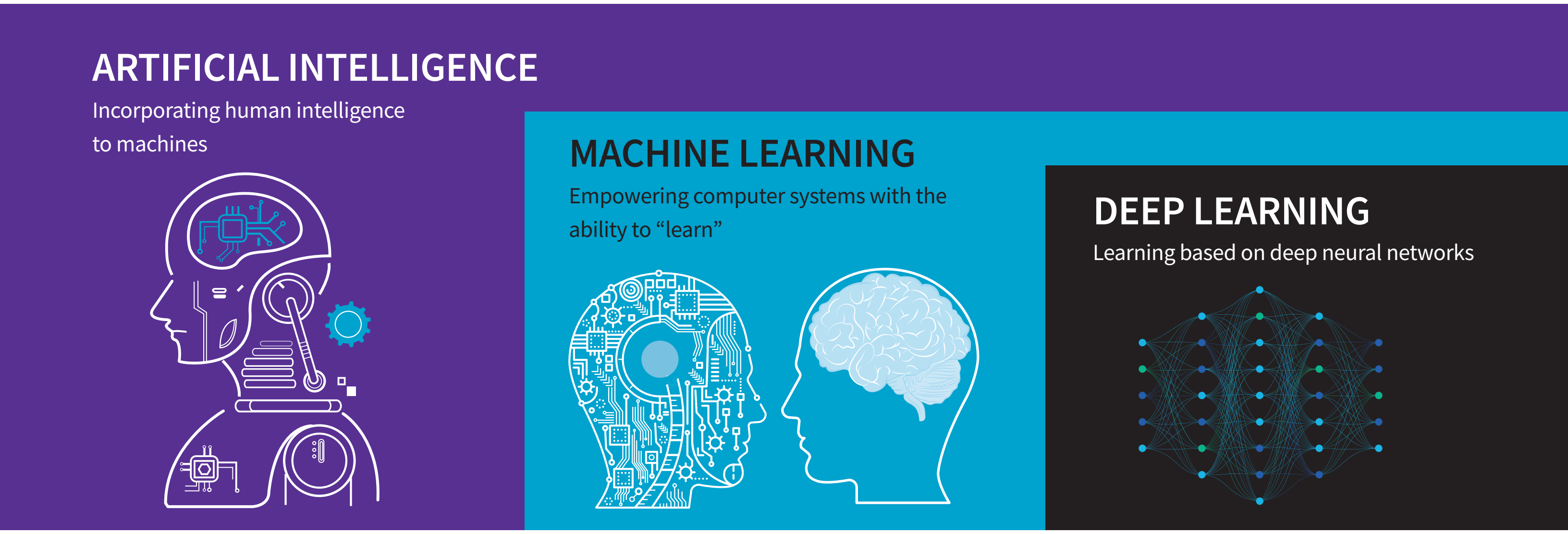

Figure 2: Artificial intelligence encompasses both machine learning and deep learning. Deep learning, a subset of machine learning, uses deep neural networks to greatly enhance its accuracy.

The Deep Learning-Based Image Reconstruction Engine

The design goal of deep learning image reconstruction is to provide a reconstructed image solution that outperforms existing model-based iterative reconstruction (MBIR) in terms of image quality, dose performance, and reconstruction speed.

To achieve this ambitious goal, the DLIR engine is designed to employ a new imaging chain that incorporates technical and clinical knowledge accumulated over the past four decades of CT.

The DLIR engine builds upon specific knowledge of the detailed design of the particular CT system. This includes knowledge of the conditioning of the collected data. Even more importantly, this knowledge is embedded within a DNN, which is capable of learning through a large number of real-world examples. Through these examples, the DLIR engine gradually optimizes the coefficients of its internal network as it figures out how to arrive at the optimal solution (i.e. the best image).

Like in the human learning process, both the training data and the training process are important to the success of the DLIR engine creation:

- Ground truth training data sets were created to establish the best training target for DLIR
- The training phase involved training, validation, and testing, before the final product is ready
- Once the DLIR engine has been trained and fully tested, the inference network uses the trained coefficients to deploy the new image reconstruction in a clinical environment

Once it is deployed, the DLIR engine is fixed to allow for a predictable outcome in the field, representative of the imaging characteristics it has learned during the supervised training phase.

Both the training data and the training process are important to the success of the DLIR engine creation.

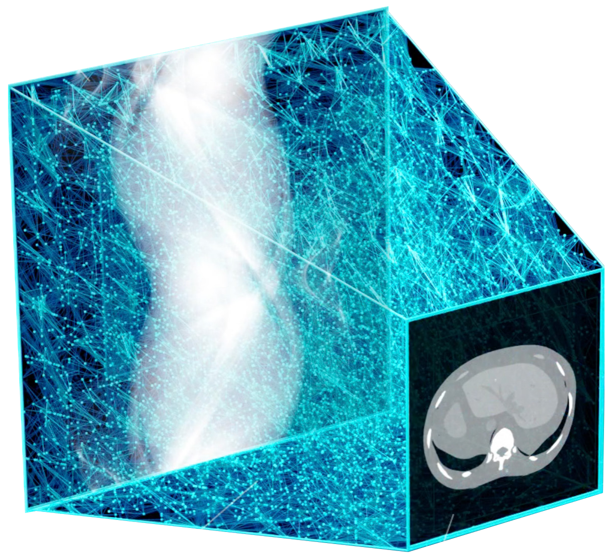

Figure 4: Schematic of the deep learning image reconstruction engine.

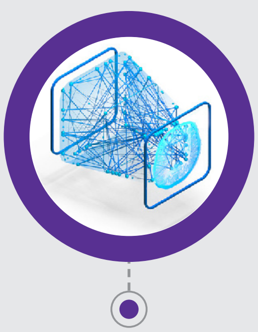

DESIGNING

Creating layers of mathematical equations, (a Deep Neural Network, DNN) that can handle millions of parameters.

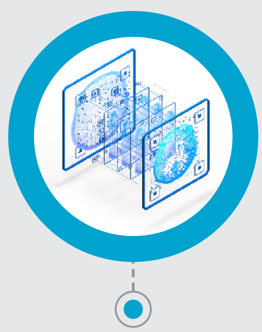

TRAINING

Inputting a low dose sinogram through the Deep Neural Network and comparing the output image to a ground truth image – a high dose version of the same data. These two images are compared across multiple parameters such as image noise, low contrast resolution, low contrast detectability, noise texture, etc. The output image reports the differences to the network via backpropagation which then strengthens some equations and weakens others and tries again. This process is repeated till there is accuracy between the output image and the ground truth image.

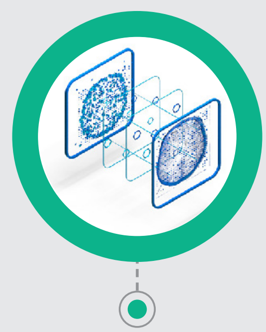

VERIFYING

The network is required to reconstruct clinical and phantom cases it has never seen before, including extremely rare cases designed to push the network to its limits, confirming its robustness.

Figure 5: Key phases of designing the deep learning image reconstruction engine.

Ground Truth Training Target

In deep learning, the training target determines the output. The target of the DLIR engine is to learn the properties of the ground truth image sets that we created.

Ground truth training data are CT images reconstructed by FBP that can faithfully represent the scanned object.

FBP is a mathematically accurate reconstruction algorithm developed under the best data acquisition and reconstruction conditions (i.e., from ideal projection data acquired with high radiation dose). After being refined over many decades, FBP has a unique advantage – when the input projection data includes low noise statistics, the output image exhibits a "natural" noise texture that is well accepted by the radiology community.

"Ideal" projection data is obtained by optimizing the data acquisition to minimize all non-ideal behaviors of the CT system, such as scatter and other degradations inherent to the physics of X-ray interaction with matter, and correcting for the residual non-idealities, such as beam hardening.

The ground truth training data are based on images collected from both phantoms in the laboratory and patients in a clinical setting, and span a variety of acquisition protocols. As a result, DLIR was trained on a massive number of patient and phantom cases that cover different body habitus and anatomies, scan conditions, and clinical indications.

Ground truth training data are CT images reconstructed by FBP that can faithfully represent the scanned object.

Supervised Training

The training process includes training, validation, and testing, which was supervised by GE HealthCare CT image quality experts and experienced radiologists.

Training starts with an objective task and selection of the training data, which includes the input data to the neural network and the corresponding expected output data. For each scanned object, both a high-dose, low-noise dataset and a low-dose, high-noise dataset are acquired. Images reconstructed with the high-dose dataset produce the ground truth. The DLIR engine is applied on the low-dose datasets to produce an estimation of the reconstructed images. Since the ground truth is known, it is used as the training target for the deep learning-based reconstruction engine.

The training process is outlined below:

- The DLIR engine generates the output image from an input sinogram that is acquired with low radiation dose
- The features of the temporary output image are compared to the ground truth image to find the differences in terms of image noise, noise texture, low-contrast resolution, high-contrast spatial resolution, and other metrics
- Millions of parameters representing the DNN are fine-tuned through embedded backpropagation based on those differences. The goal of this parameter optimization is to reduce the difference between the DLIR output and the ground truth images
- The above training process is repeated on thousands of training data until the DLIR engine can generate output images to accurately match the ground truth images in a large variety of realistic conditions
- The DLIR engine then undergoes extensive testing whereby a large number of validation datasets that were not used in the training are reconstructed to ensure the robustness and accuracy of the DLIR engine

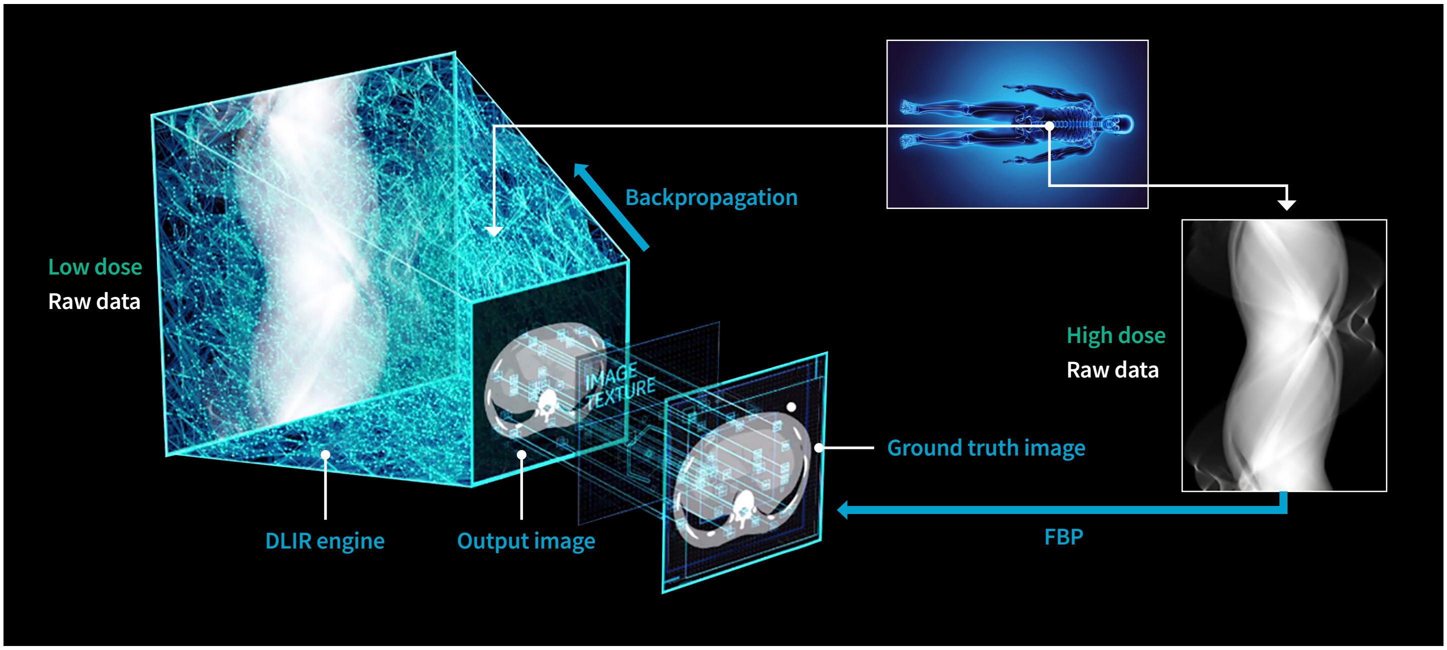

Figure 6: A schematic of training process.

One of the key criteria of a successful training is the quality of the generated images. Compared to FBP images generated from the same scan data, DLIR images not only need to successfully remove noise, but also preserve noise texture, and anatomical and pathological details. This requirement forces the DLIR to undergo rigorous validation and testing. The validation and testing process required that the DLIR engine reconstruct numerous cases that it had never seen before, and many corner conditions, cases that are extremely rare and were specially designed to challenge the algorithm. To demonstrate the robustness of the DLIR algorithm, Figure 7 depicts images generated with the same scan data: the image on the left was reconstructed with FBP algorithm, the image in the middle was reconstructed with DLIR, and the image on the right was generated by subtracting DLIR image from the FBP image. The fact that anatomical structure is not present in the difference image, even for such complex anatomy with both low-contrast and high-contrast detail, is a clear demonstration of the robustness of DLIR.

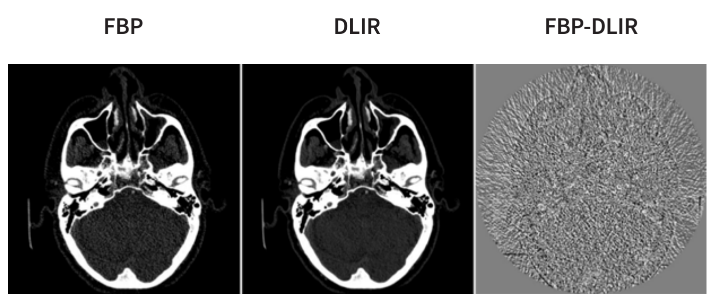

Figure 7: Clinical images to demonstrate the robustness of DLIR algorithm.

The training process includes training, validation and testing which was supervised by GE CT image quality experts and experienced radiologists.

A key criterion of successful training is for output images to not only successfully remove noise but also preserve noise texture, anatomical and pathological details, compared to the ground truth training target.

Inferencing and Deployment

Inferencing is a term used widely in the deep-learning community that essentially means using the trained neural network in practice. Unlike training, it doesn't include a backward pass to compute error and update weights. It takes a network that has already been trained and uses that trained model to perform useful tasks.

After the completion of supervised training, the DNN-based DLIR engine has been formulated with all parameters pre-computed and fixed, and is able to generate ground truth equivalent high-quality DICOM images – commercially known as TrueFidelity DL CT images.

The DLIR engine is deployed to run natively on the reconstruction hardware of specific CT systems. The scan data acquired by the CT scanner goes through the DLIR engine only once to produce the TrueFidelity DL images (Figure 8). As examples shown in Figure 9, the resultant reconstruction throughput is fast enough for routine CT use, even in acute care settings.

DLIR provides three selectable reconstruction strength levels (low, medium, high) to control the amount of noise reduction. Without impacting reconstruction speed, the strength levels are selectable and can be built into the reconstruction protocols based on the clinical applications and radiologist preference.

At the completion of training, the DLIR engine can generate TrueFidelity DL CT images with fast reconstruction speed for routine CT use.

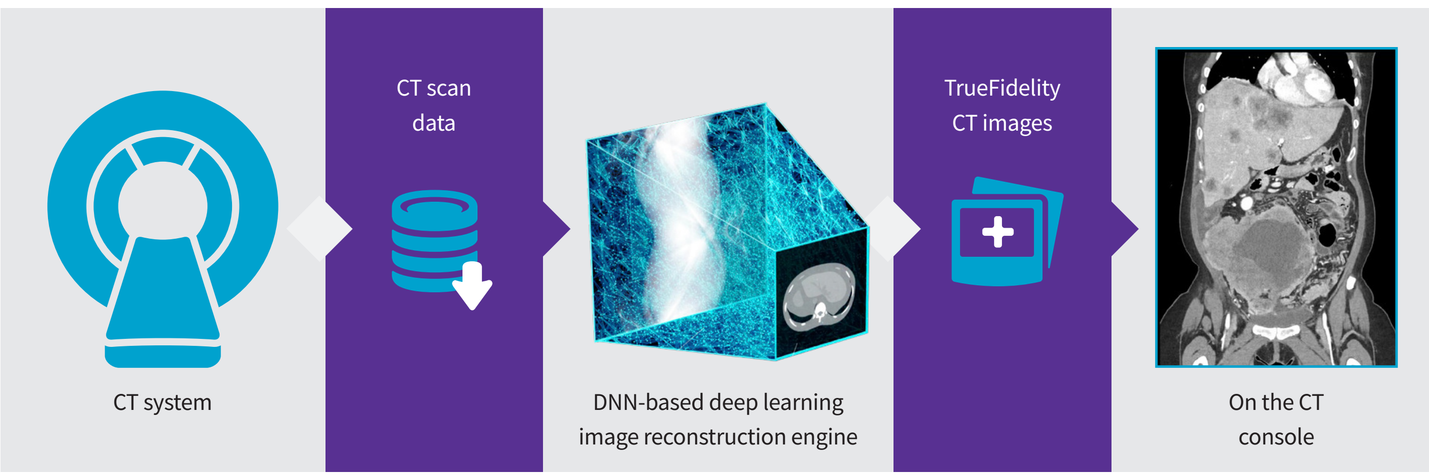

Figure 8: Reconstruction flow of deep learning image reconstruction.

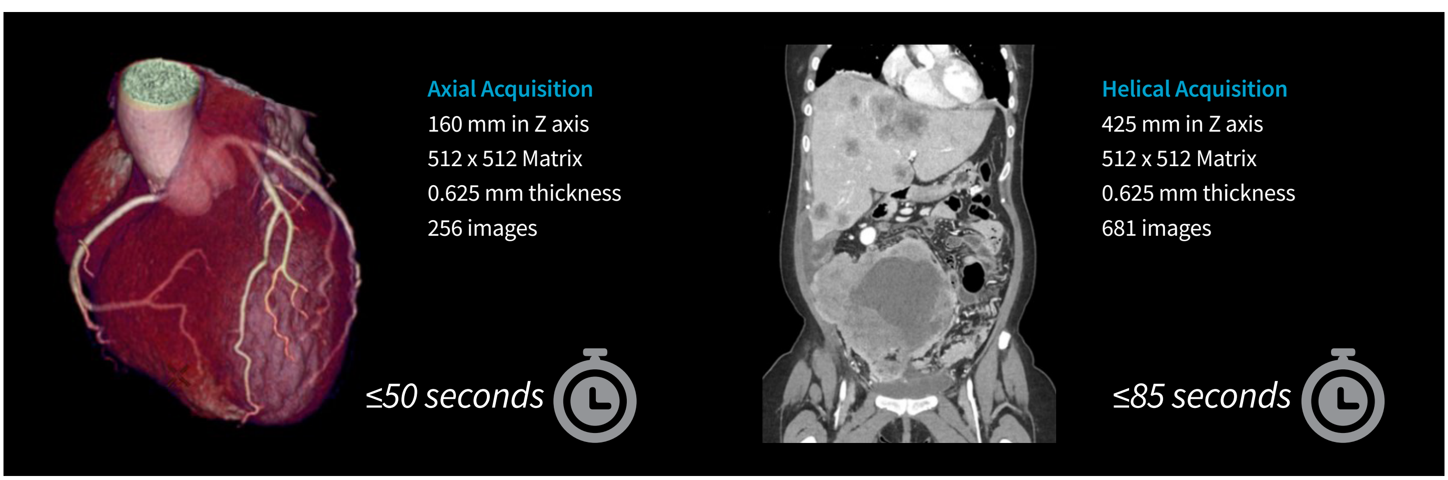

Figure 9: Examples of reconstruction speed of deep learning image reconstruction.

Early Evidence: Phantom Studies

Phantom studies were designed to evaluate the performance of TrueFidelity DL on image noise reduction (Fig. 10), noise texture (Fig. 11), contrast-noise-ratio improvement (Fig. 12), and low contrast detectability improvement (Fig. 13).

Figure 10: Evaluation of Image Noise Reduction

The Catphan® 600 phantom (The Phantom Laboratory, NY, US) is combined here with a 25*35 cm oval body annulus to simulate a typical adult body. The phantom's uniform section (CTP486) was scanned on Revolution CT with 120 kV, CTDIvol = 3.27 mGy. Images were reconstructed with 0.625 mm thickness using FBP, ASiR-V 50%, DLIR-L/M/H. The image noise (standard deviation in CT number in a uniform region of interest) was measured with a 4 cm* 4 cm ROI in the center of the image.

Measured CT number standard deviation values, shown in (Fig. 10a), show that DLIR has better noise reduction performance than FBP and ASiR-V. The relative noise reduction with the baseline of FBP (Fig. 10b) illustrates a progressive image noise reduction as DLIR strength increases.

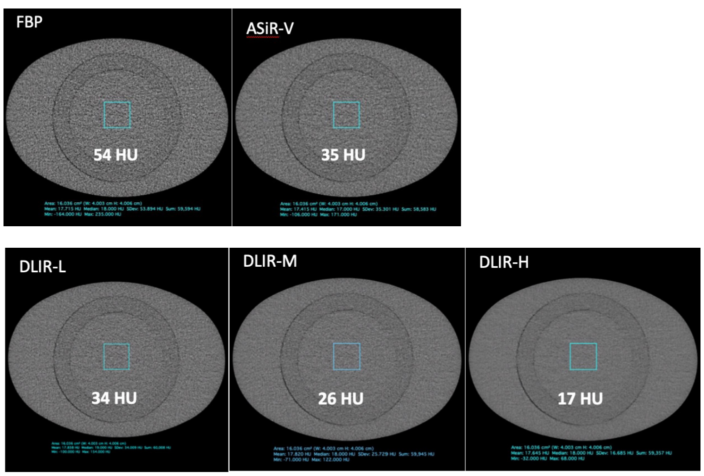

Figure 10a.

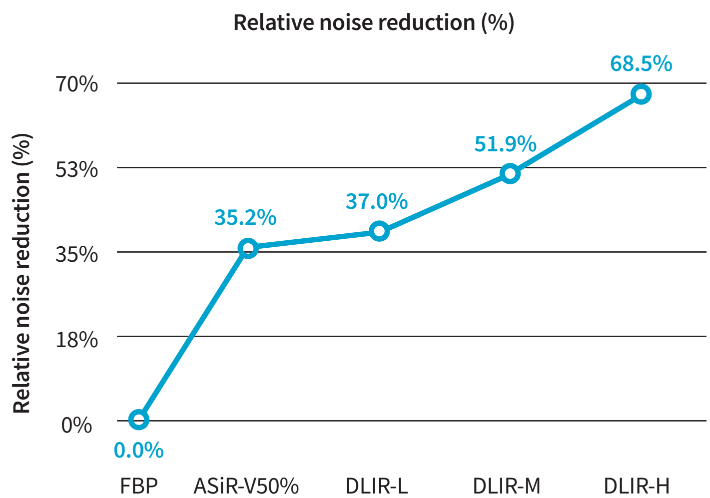

Figure 10b.

Figure 11: Evaluation of Noise Texture via Noise Power Spectrum

The DLIR engine is trained to create TrueFidelity DL CT images with a noise texture similar to high dose FBP.

Noise texture can be characterized by the noise power spectrum (NPS).[8] NPS is a widely used metric for the characterization of noise patterns in CT images.[9-13] It describes the noise power within a chosen region-of-interest (ROI) as a function of spatial frequency. When the noise power peaks at lower frequencies the image is observed to have coarse noise granularity, and when it peaks at higher frequencies it is observed to have finer noise granularity.[9,11] The normalized NPS (nNPS), whereby the NPS is normalized by the area under the curve, is a fair method for comparing acquisitions with different dose levels.

The 20 cm water phantom (GE HealthCare, WI, US) was scanned on Revolution CT with two CTDIvol levels: 4.9mGy and 15.1mGy, and 2.5 mm thick images were reconstructed using FBP, ASiR-V 100% and DLIR-H (Fig. 11a). ASiR-V 100% and DLIR-H were selected for the highest potential visible change in image texture relative to the FBP reference at higher dose, for a challenging setup to compare the impact of the iterative reconstruction and deep-learning technologies on image appearance. The normalized NPS curves (Fig. 11b) show that images of low-dose DLIR have the same NPS characteristics as the images of high-dose FBP, whereas iterative reconstruction produces results that are clearly different.

FBP, 15.1 mGy **ASiR-V 100%, 4.9 mGy** **DLIR-H, 4.9 mGy**

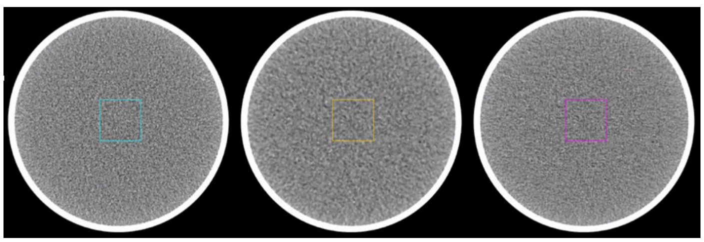

Figure 11a.

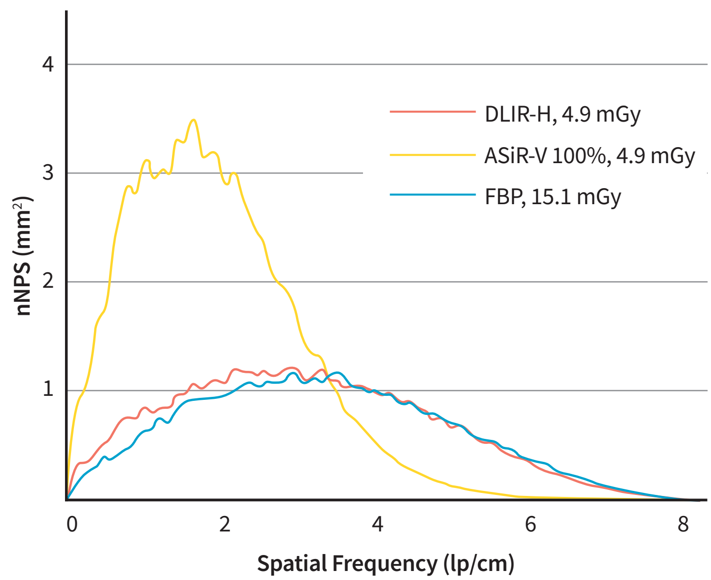

Figure 11b.

Figure 12: Evaluation of Contrast-to-Noise Ratio (CNR) Improvement

The ACR 464 phantom (Gammex, WI, US) was scanned on Revolution CT with 120 kV, CTDIvol = 8.5 mGy and reconstructed with FBP, ASiR-V and DLIR L/M/H. The phantom Module-2 features a series of cylinders with different diameters ranging from 2 mm to 25 mm, all at 6HU difference from the background material, as illustrated in (Fig. 12a).

The CNR was calculated based on two ROIs of 100 mm 2 in different regions, as shown in (Fig. 12b), and consistent with ACR accreditation testing.

The CNR was calculated as

$$CNR = (Mean[ROI_1]\text{-}Mean[ROI_2])/(SD[ROI_1]),$$

where mean and SD denote mean and standard deviation in CT values inside the corresponding ROIs.[14]

Both measured CNR (Fig. 12c) and normalized CNR (Fig. 12d) demonstrates that DLIR delivers up to 2X higher CNR than FBP, and CNR increases as a function of DLIR strength.

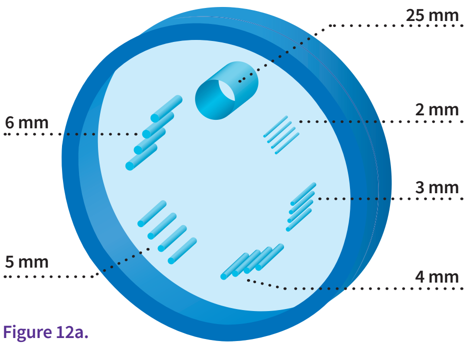

Figure 12a.

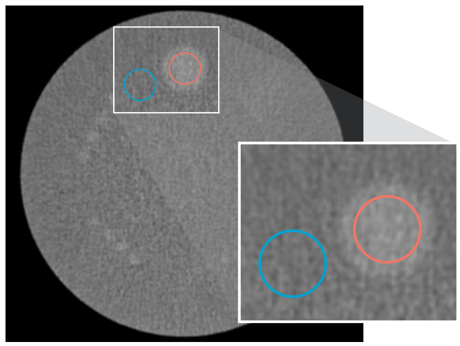

Figure 12b.

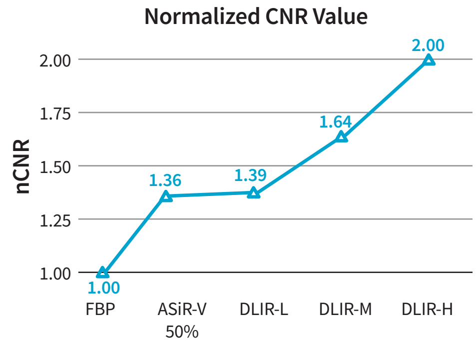

Figure 12d.

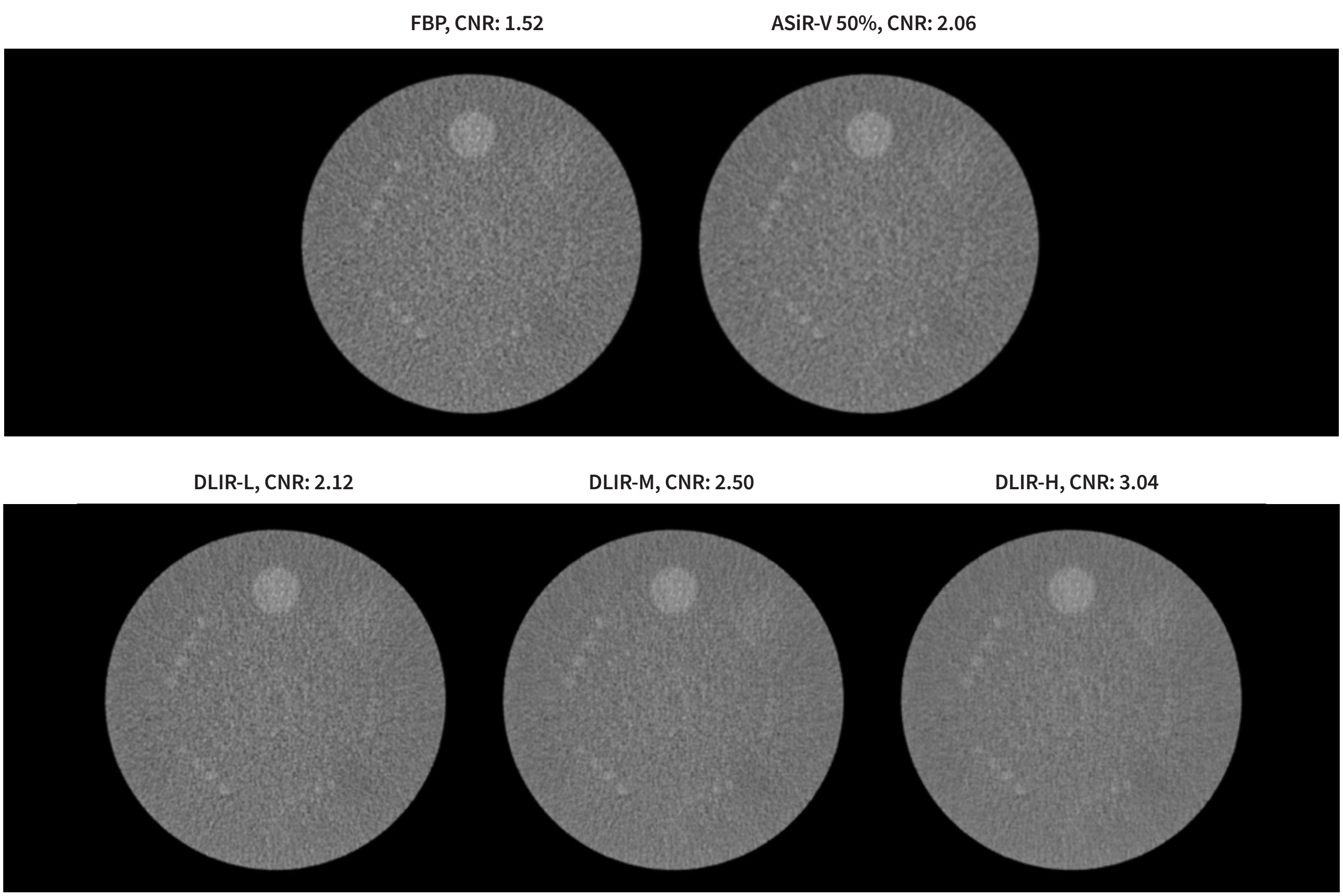

Figure 12c.

Figure 13: Evaluation of Low Contrast Detectability Improvement

Low-contrast detectability (LCD) is crucial for some CT applications, for example, liver oncology imaging where neoplastic disease commonly manifests itself as a low-attenuating object within a background of slightly higher attenuation liver tissue.

The LCD performance of DLIR was evaluated using a mathematical model observer's method, recommended by the Joint MITA-FDA CT Image Quality Task Group to evaluate CT dose and image quality. Compared to a conventional human observer method, this method is objective and consistent, and correlates well with human observer results for clinically relevant scenarios.[15]

The Channelized Hotelling Observer (CHO)1 was chosen for DLIR's LCD assessment. Receiver Operating Characteristic (ROC) curves and the Area Under the ROC Curve (AUC) values were used for LCD performance evaluation.

The Catphan 189 MITA Low Contrast Phantom (The Phantom Laboratary, NY, US) was imaged on Revolution CT with 120 kV, CTDIvol = 3.63 mGy and 4.72 mGy. This phantom (Fig. 13a) includes different low contrast objects of various sizes and intensities (Fig. 13b). The phantom scans were reconstructed with ASiR-V 100% and DLIR-H.

Fig. 13c provides plots of the model observer ROC curves and AUC values and their associated error bars. The blue and green curves represent the ROC curves of ASiR-V and DLIR, respectively. The higher the true positive fraction the better the low contrast detection. The blue and green bars represent ASiR-V 100% and DLIR-H, respectively. The higher the AUC value the better the LCD performance.

Both ROC curves and AUC values demonstrate that DLIR outperforms ASiR-V in low contrast detectability.

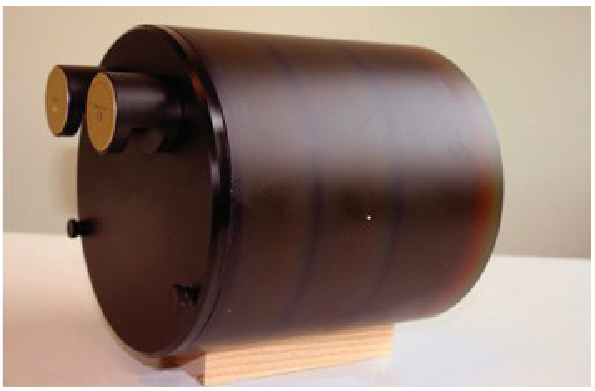

Figure 13a.

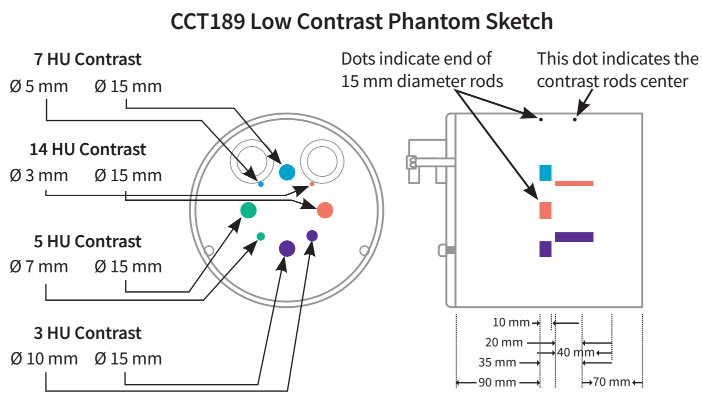

Figure 13b.

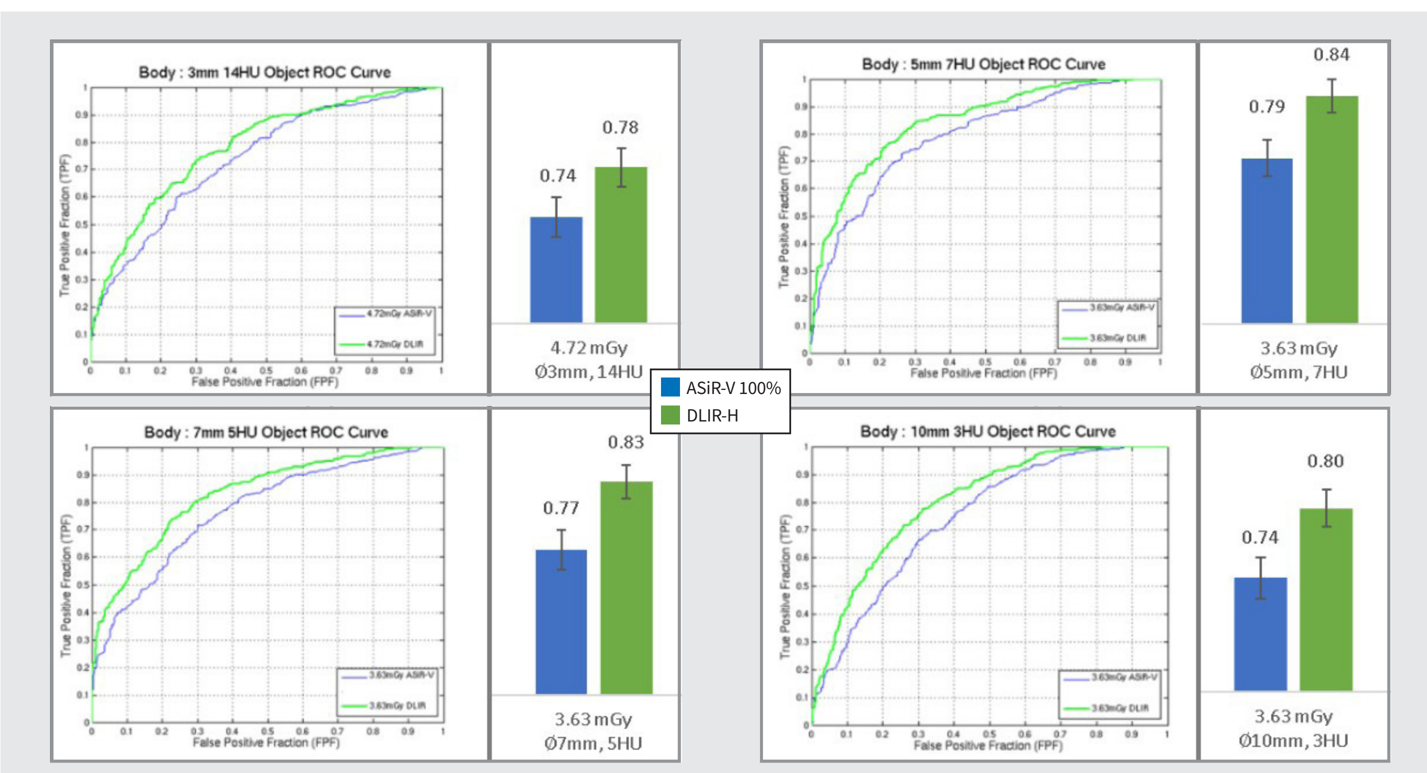

Figure 13c.

Early Evidence: Clinical Cases

Deep learning image reconstruction (DLIR) has been cleared by FDA for different anatomies with patients of all ages with all ages, including head, whole body, and cardiovascular applications. DLIR's different levels (low, medium and high) can be used for different clinical tasks to improve image quality. The following clinical cases (Fig. 14 – 19) demonstrate how early adopters use DLIR to improve patient care.

Figure 14: Abdominal and Pelvic Imaging

Example of TrueFidelity DL CT images in abdominal and pelvic CT imaging. The patient with multiple metastatic cancer lesions was scanned on Revolution CT, images were reconstructed with 0.625mm thickness using FBP(A,D,G), ASiR-V (B,E,H) and DLIR(C,F,I).

In axial, coronal and sagittal planes, DLIR demonstrates similar performance in reducing image noise, preserving noise texture and better visualizing the boundaries and internal structures of cancer lesions.

Scan type	Helical
Rotation time, s	0.5
Pitch	1.375
kV	120
mA	Smart mA
Slice, mm	0.625
Noise index	13
CTDIvol, mGy	6.7
DLP, mGy-cm	311
Eff. dose, mSv	4.7
k, *DLP	0.015

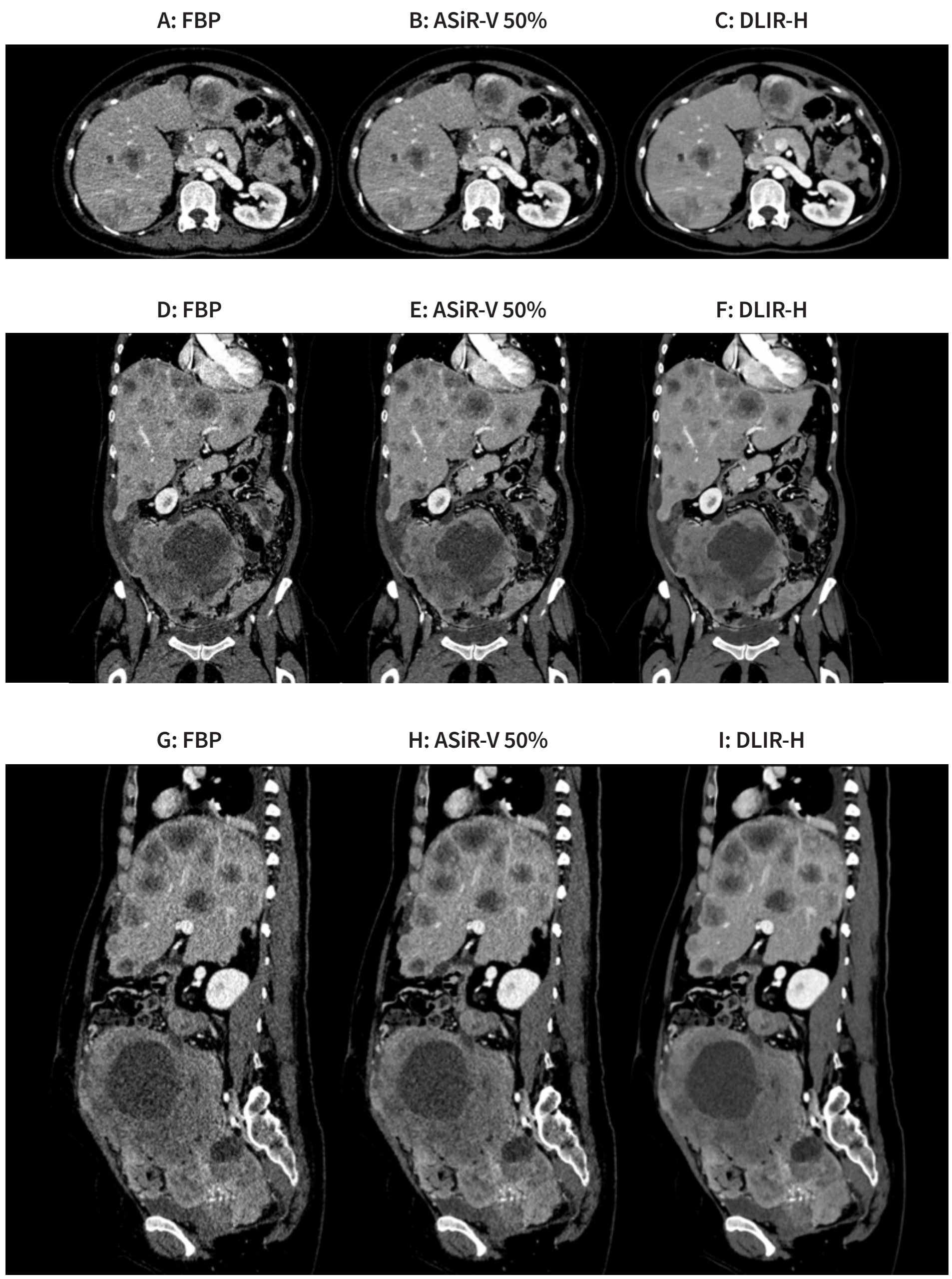

Figure 15: Head Imaging

Example of TrueFidelity DL CT images in neuro CT imaging. The patient was scanned at 120 kV, 330 mA, with recorded radiation exposure of CTDIvol = 49.5 mGy. Images were reconstructed with 2.5 mm thickness using FBP(A), ASiR-V (B) and DLIR (C). DLIR images show decreased image noise, improved noise texture and grey/white matter differentiation.

Courtesy of University Hospital Jena, Germany.

Scan type	Axial
Rotation time, s	1.0
Slice, mm	2.5
kV	120
mA	330
Noise index	3.4
CTDIvol, mGy	49.5
DLP, mGy-cm	694
Eff. dose, mSv	1.45
k, *DLP	0.0021

A: FBP **B: ASiR-V 50%** **C: DLIR-H**

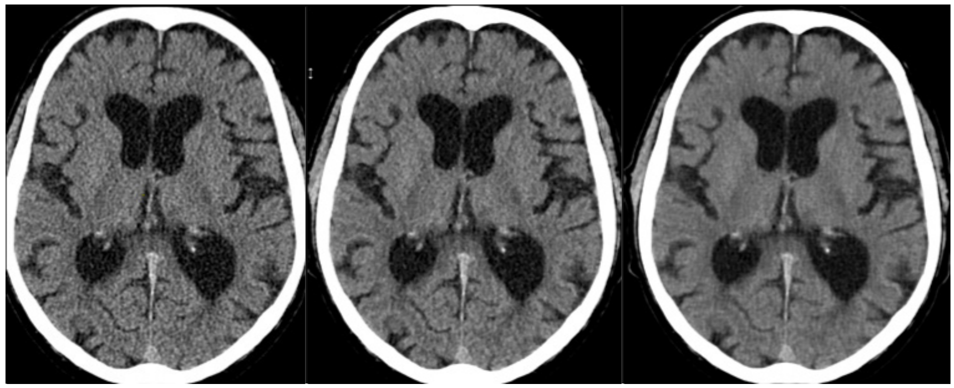

Figure 16: Cardiovascular Imaging

Example of TrueFidelity DL CT images in coronary CT angiography. DLIR used with cardiac high-resolution protocol for imaging the coronary arteries with calcified and soft plaque. Images reconstructed with DLIR (C, F-I) exhibited image quality improvement with reduced image noise, better defined anatomical edges and borders and enhanced visualization of fine details, when compared with FBP(A, D) and ASiR-V(B, E).

Courtesy of the Centre Cardiologique du Nord, France.

Scan type	1-beat cardiac axial
Rotation time, s	0.28
Slice, mm	0.625
kV	100
mA	580
Kernel	HD STD
CTDIvol, mGy	4.54
DLP, mGy-cm	63.6
Eff. dose, mSv	0.89
k, *DLP	0.014

A: FBP

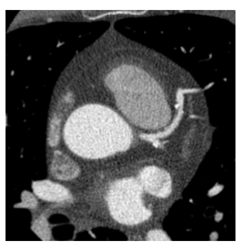

B: ASiR-V 50%

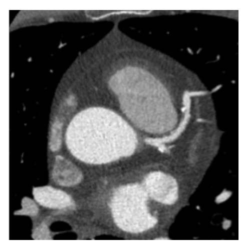

C: DLIR-H

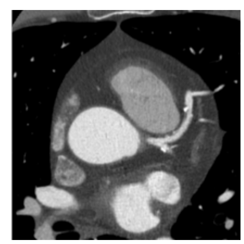

D: FBP

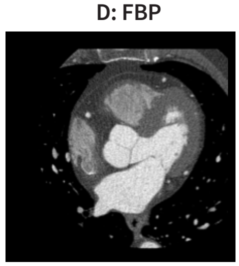

E: ASiR-V 50%

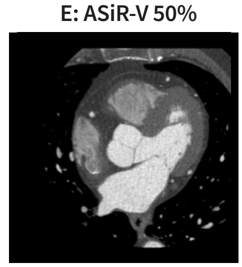

F: DLIR-H

G: DLIR-H

H:DLIR-H

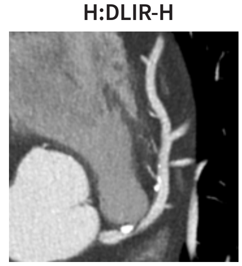

I:DLIR-H

Figure 17: Thoracic Imaging

Example of TrueFidelity DL CT images in thoracic CT imaging. The patient has a history of pneumothorax and bronchiectasis, and has difficulty holding their breath. The whole chest was scanned within 1.2 s on Revolution CT using HyperDrive (a high pitch helical scan mode). Images were reconstructed with 0.625 mm thickness using FBP(A), ASiR-V (B), and DLIR-M(C,D).

DLIR significantly reduces image noise and improves visualization of anatomical and pathological details to reveal moderate left pneumothorax, bilateral bronchiectasis with fibrosis and consolidation in right upper lobe.

Courtesy of Froedtert and Medical College of Wisconsin, USA.

Scan type	HyperDrive
Rotation time, s	0.5
Pitch	1.531
Slice, mm	0.625
Scan length, mm	330
Scan time, s	1.2
kV	100
mA	202 – 387
Noise index	19.4
CTDIvol, mGy	4.4
DLP, mGy-cm	194
Eff. dose, mSv	2.7
k, *DLP	0.014

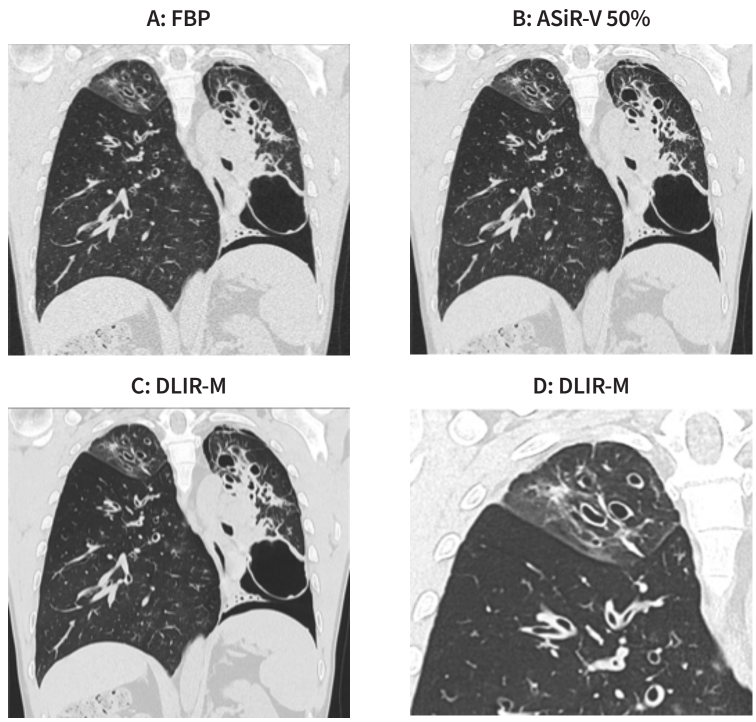

Figure 18: Metal Artifact Reduction

DLIR works synergistically with Metal Artifact Reduction (Smart MAR). The exam was completed in less than 1s on Revolution CT using HyperDrive (a high pitch helical scan mode). DLIR and Smart MAR work together to improve image quality and reveal hidden anatomical structure by removing metal artifacts.

Courtesy of Froedtert and Medical College of Wisconsin, USA.

Scan type	HyperDrive
Rotation time, s	0.35
Pitch	1.531
Slice, mm	0.625
Scan length, mm	370
Scan time, s	1
kV	140
mA	215 – 382
Noise index	11.4
CTDIvol, mGy	6.7
DLP, mGy-cm	315
Eff. dose, mSv	4.7
k, *DLP	0.015

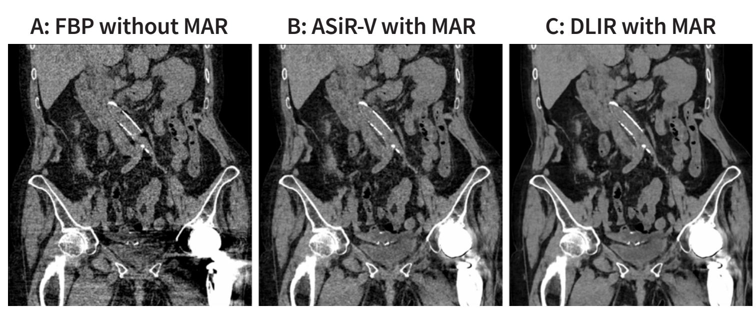

Figure 19: Oncology Follow-up Scan with Lower Dose

This example shows images of an oncology patient (BMI = 33) who underwent two different CT scans: a prior standard dose CT protocol and a follow-up lower dose CT protocol. Images (A,C) are the venous phase of the prior scan reconstructed with ASIR-V 50%; images (B,D) are the venous phase of the follow-up scan reconstructed with DLIR-H. DLIR demonstrated improved image quality with 51% lower radiation dose.

Courtesy of University Hospital Jena, Germany.

	Prior exam	Follow-up exam
Scan type	Helical	Helical
Rotation time, s	0.5	0.5
Pitch	1	1
Slice, mm	0.625	0.625
kV	120	120
mA	Smart mA	Smart mA
Noise index	27	35
CTDIvol, mGy	Non-contrast: 10.38 Arterial: 10.50 Venous: 10.38	Non-contrast: 4.54 Arterial: 4.80 Venous: 5.1

A: ASiR-V 50%
Prior exam with 10.38 mGy

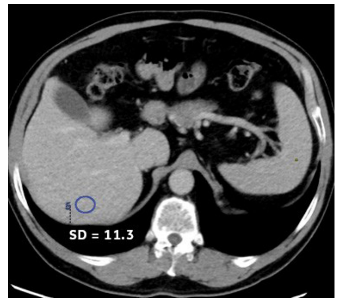

B: DLIR-H
Follow-up exam with 5.1 mGy

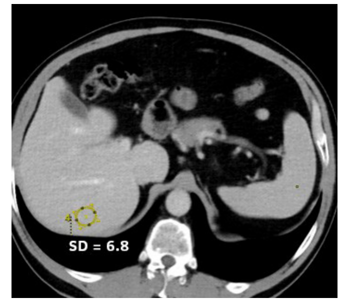

C: ASiR-V 50%
Prior exam with 10.38 mGy

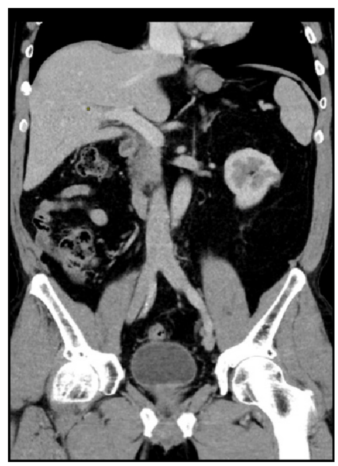

D: DLIR-H
Follow-up exam with 5.1 mGy

Conclusion

The era of deep learning-based CT image reconstruction has arrived in clinical practice. With an innovative design and advanced training method, GE HealthCare's deep learning image reconstruction produces intelligent image noise reduction and restores preferred noise texture, leading to improved objective and subjective image quality compared to filtered back-projection and iterative reconstruction.

The resultant TrueFidelity DL images improve image quality in previously challenging areas, such as low-dose imaging, high-resolution imaging, and the evaluation of obese individuals. It also holds the potential to enable designing CT acquisition protocols at reduced radiation dose levels without sacrificing image quality, which is particularly attractive in screening examinations, pediatric imaging, and for repeat examinations.

More evidence-based physics and clinical studies are needed to evaluate all aspects of this emerging technology and to enhance its clinical adoption to improve patient care.

Glossary

Artificial Intelligence (AI)
A broad term to cover the theory and development of computer systems able to perform tasks that normally require human intelligence.

Backpropagation
The central mechanism by which deep neural networks can learn. It is the messenger telling the network whether or not the network made a prediction with imperfect results. In the context of learning, backpropagation commonly uses the gradient descent optimization algorithm to adjust the weight of neurons by calculating the gradient of the loss function.

Deep learning (DL)
A subset of machine learning, DL utilizes deep neural networks which consist of layers of mathematical equations and millions of connections and parameters that get trained and strengthened based on the desired output.

Deep learning image reconstruction
A CT image reconstruction technique that utilizes deep neural networks to generate CT images.

Deep neural network (DNN)
An artificial neural network with multiple layers of mathematical equations and millions of connections and parameters that get trained and strengthened based on the desired output.

DLIR-low/medium/high
Three selectable reconstruction strength levels (Low, Medium, High) to control the amount of noise reduction. Without impacting reconstruction speed, the strength levels are selectable and can be built into reconstruction protocols based on the clinical applications and radiologist preference.

Ground truth training data
Refers to millions of CT images reconstructed by FBP that faithfully represent the scanned object, and that are used to train the DLIR engine to generate TrueFidelity CT images.

Inferencing
Using the trained neural network in practice. Unlike training, it doesn't include backpropagation to compute the error and update the DNN weights. It takes a network that has already been trained and uses that trained model to perform useful tasks.

Machine learning (ML)
A branch of artificial intelligence based on the idea that systems can learn from data, patterns, and features to make decisions with minimal human intervention.

Mathematical model observer method
An objective method to evaluate low contrast detectability, which is recommended by MITA-FDA CT Image Quality Task Group.

Noise power spectrum (NPS)
A widely used metric for the characterization of noise patterns in CT images. It describes the noise texture within a chosen region-of-interest as a function of spatial frequency.

TrueFidelity deep learning image reconstruction
A GE HealthCare designed, FDA cleared, deep neural network based CT image reconstruction technology to generate TrueFidelity CT images with outstanding image quality and preferred image noise texture.

TrueFidelity CT Images
The commercial name of high-quality CT images generated by GE HealthCare's deep learning image reconstruction engine.

References

1. Willemink, M. J., & Noël, P. B. (2018). "The evolution of image reconstruction for CT – from filtered back projection to artificial intelligence." *European Radiology*, 46 (Suppl 2), 1–11.
2. J. Hsieh. "Adaptive statistical iterative reconstruction." *White Paper*, GE HealthCare (2008).
3. Jiahua Fan, Meghan Yue, and Roman Melnyk, "Benefits of ASiR-V Reconstruction for Reducing Patient Radiation Dose and Preserving Diagnostic Quality in CT Exams." *White Paper*, GE HealthCare (2014).
4. J. B. Thibault, K. D. Sauer, C. A. Bouman, and J. Hsieh, "A three-dimensional statistical approach to improve image quality for multislice helical CT." *Med. Phys.* 34(11), 4526-4543 (2007).
5. Geyer, L. L., Schoepf, U. J., Meinel, F. G., Nance, J. W., Jr, Bastarrika, G., Leipsic, J. A., et al. (2015). "State of the Art: Iterative CT Reconstruction Techniques." *Radiology*, 276(2), 339–357.
6. LeCun, Y., Bengio, Y., & Hinton, G. (2015). *Deep learning*, 521(7553), 436–444.
7. Chartrand, G., Cheng, P. M., Vorontsov, E., Drozdzal, M., Turcotte, S., Pal, C. J., et al. (2017). "Deep Learning: A Primer for Radiologists." *RadioGraphics*, 37(7), 2113–2131.
8. Bushberg et al., "The Essential Physics of Medical imaging, Third Edition." *Lippincott, Williams, and Wilkins* (2013), p.86.
9. Solomon et al., "Quantitative comparison of noise texture across CT scanners from different manufacturers." *Medical physics* 39 (2012): 6048-55.
10. Andersen et al. "Image quality with iterative reconstruction techniques in CT of the lungs – A phantom study." *European Journal of Radiology Open*. 5 (2018): 35-40.
11. Boedeker et al., "Application of the noise power spectrum in modern diagnostic CT (MDCT): part I. Measurement of noise power spectra and noise equivalent quanta." *Physics in Medicine and Biology*. 52 14 (2007): 4027-46.
12. Baek J, Pelc NJ., "The noise power spectrum in CT with direct fan beam Reconstruction." *Medical Physics*. 37 5 (2010): 2074-81.
13. Morsbach et al., "Noise Texture Deviation: A Measure for Quantifying Artifacts in Computed Tomography Images with Iterative Reconstructions." *Investigative Radiology*. 52 2 (2017): 87-94.
14. "Radiology, A. C. O." *American College of Radiology CT Accreditation Program testing instructions* (2015).
15. Barrett, H. and Myers, K., "Foundations of Image Science," *John Wiley & Sons* (2004).

November 2023

JB68676XX

GE HealthCare